TOWARDS CONTACTLESS SKID RESISTANCE MEASUREMENT

Andreas Ueckermann, Dawei Wang
Institute of Highway Engineering, RWTH Aachen University

Corresponding author:
Andreas Ueckermann, RWTH Aachen University, Institute of Highway Engineering, Mies-van-der-Rohe-Str. 1, D-52074 Aachen

ABSTRACT

Monitoring of skid resistance is an important component of maintaining road networks. Over the past decades a wide range of routine measurement devices has been developed, all of them measuring the friction force between a rubber wheel and the (wetted) road surface. At the same time many efforts have been undertaken on a variety of grounds to predict skid resistance solely from texture measurements. We present a concept of contactless skid resistance measurement which is based on optical texture measurement and consists of two components:

1) measurement of the pavement texture by means of an optical measuring system and
2) calculation of the skid resistance based on the measured texture by means of a rubber friction model.

We describe the basic assumptions underlying the theoretical approach and present the model based on the theory of Persson. Two skid resistance measuring devices are chosen to prove the theoretical approach: one laboratory device called Wehner/Schulze (W/S) machine which corresponds to a blocked-wheel braking test and the ViaFriction device of ViaTech AS which measures the skid resistance under controlled longitudinal slip and corresponds to ABS braking conditions. We describe the measurement devices and experiments conducted. The results are very promising although in the case of the ViaFriction device only a few surfaces could be tested. A close relation between measured and predicted friction coefficients could be found. The 95 % prediction interval is +/- 0.04 and the variance 0.02. Thus, a strong indication could be provided that skid resistance could be measured without contact in the future.

1. INTRODUCTION

Monitoring of skid resistance is an important component of maintaining road networks. Over the past decades a wide range of routine measurement devices (with just as many different measures of skid resistance) has been developed, all of them measuring the friction force between a rubber wheel and the (wetted) road surface. At the same time many efforts have been undertaken on a variety of grounds to predict skid resistance solely from texture measurements since it is known for long that skid resistance (besides other factors like operating-, tire- and environmental factors) largely depends on pavement texture, especially on its fine-scale components below one millimeter. Recent advances are reported in *(1-3)* where skid resistance is predicted from parameters directly extracted from images of the road surface. Many approaches use 2-dimensional or 3-dimensional topographical data of the surface collected by means of laser displacement sensors or laser profile scanners *(4-9)*. Topographical data can also be generated by stereoscopic imaging. Although not new in the application to pavement texture analysis *(10,11)* recent work on algorithms for the extraction of surface topography from image and the assessment of surface roughness by means of image-based descriptors is described in *(12-14)*. Light scattering methods based on depolarization *(15,16)* or back-scattering pattern analysis *(17,18)* have been proposed in the past but obviously not persued, presumably because it is believed that optical pavement properties not necessarily reflect tire-pavement interaction.

Basically, three approaches to predict skid resistance from road surface data can be found in (recent) literature: 1) prediction through texture (or texture-related) parameters, which correlate with rubber friction, 2) prediction through modeling of rubber contact and rubber friction (partially including the lubricant), and 3) a combined approach comprising both, texture indicators and physical modeling, as described e.g. in *(19-21)*. The first approach can involve statistical (regression) models *(22-24)*, fuzzy-logic *(25)* and artificial neural networks *(5,7)*. The second one largely focuses on hysteresis friction since hysteresis is the dominating mechanism during braking on wet road pavements. However, other phenomena like adhesion and the influence of water in the tyre/road interface are dealt with as well in related papers.

2. FACTORS INFLUENCING SKID RESISTANCE

It is widely acknowledged that the microtexture (wavelengths below 0.5 mm) governs the peak value of the (wet) friction coefficient – slip (or sliding speed) curve whereas the macrotexture (wavelengths between 0.5 and 50 mm) governs its decrease (Figure 1). The lower the macrotexture the steeper the decrease, or, in other words, an adequate macrotexture (which means a high water drainage capacity) is necessary to assure road safety over a wide range of

speeds. Size, density and shape (slope) of the microasperities on top of the aggregates are essential to overcome the thin water film and to make direct contact with the rubber. A close relationship between friction coefficient and the average slope of the microasperities in the contact zone can be observed and mathematically explained *(26)*.

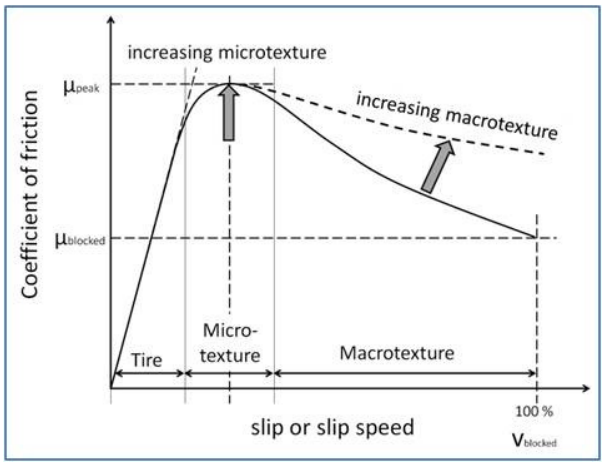

Figure 1 Main factors governing the friction coefficient – sliding speed curve

When skid resistance is measured, let's say with a measuring speed of 60 km/h and a fixed slip of 20%, only a part of the measured slip speed (which would be 12 km/h in this case) is due to actual sliding, the other one is due to deformation of tread elements as demonstrated in Fig. 2. The amount of deformation slip depends on the tire stiffness: a blank, "stiff" tire would exhibit only little deformation implying that the measured slip speed almost equals the actual slip speed, whereas a treaded tire would undergo a higher deformation, depending on the elasticity of the tread rubber and the geometry of the tread pattern. It should be noted that the slip speed according to Figure 2 is just a mean value averaged over the contact length and thus a simplification of the real slip conditions within the contact area.

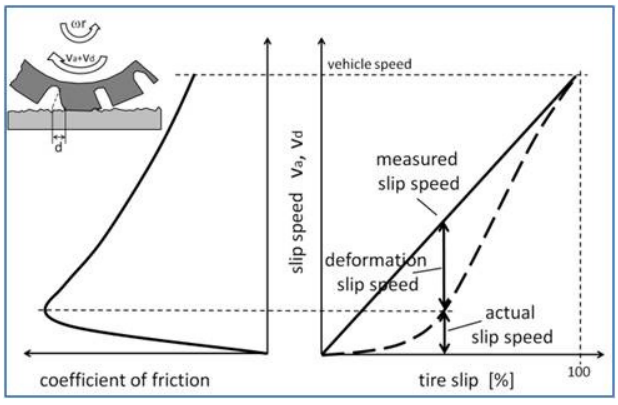

Figure 2 Tire friction and slip speed (from *(27,28)*)

A three-zone model according to Moore *(29)* can help to illustrate the contact conditions in the tire-road interface during rolling or skidding on a wet surface from a tribology point of view (Figure 3). Zone A is the “sinkage” or “squeeze-film” zone and corresponds to the “elasto-hydrodynamic lubrication” regime where the water completely separates the two surfaces. Zone B is the “draping” or “transition” zone and corresponds to the “mixed lubrication” regime where the tread elements, having penetrated the squeeze-film, commence to “drape” over the major asperities. Zone C is the actual contact or traction zone and corresponds to the “boundary lubrication” regime where in parts dry contact can be established. The lengths of the zones depend on vehicle speed and the amount of water that has to be expelled from the interface. Due to partly the lubricant and partly the sliding velocity used in skid resistance measurements adhesion is largely inhibited and hysteretic friction the dominant friction mechanism.

Several models have been derived in the past to describe the influence of the lubricant on the friction coefficient. Empirical approaches used within the context of harmonizing skid resistance measurements include the water influence indirectly by an exponential function characterized by a speed factor which again is dependent on the macrotexture. Different functions have been proposed to describe the speed dependance, more recently in *(30)* where the function is derived from the Stribeck curve (Figure 4) which describes the friction as a function of speed (or a lubrication parameter) and different lubrication regimes. The zones in Figure 4 correspond to the zones in Figure 3.

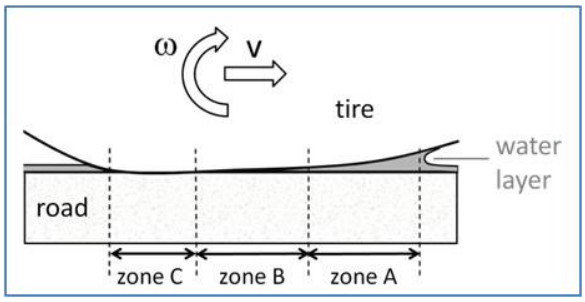

Figure 3 Three zone model according to Moore (29)

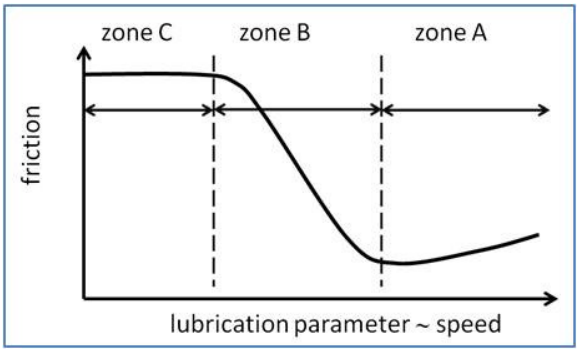

Figure 4 Stribeck curve and lubrication regimes *(30)*

In spite of the extensive knowledge on the relationship between pavement texture and wet skid behavior gained over the past decades, a reliable method to predict skid resistance solely from texture measurements is still missing. It remains a challenging task to combine the measurement of microtexture under routine monitoring conditions with appropriate algorithms that consider the complex mechanisms involved in tyre/road interaction to a reliable measuring technique that can be applied to the whole range of pavements in a road network.

This paper is intended to make a contribution to contactless skid resistance measurement. It deals with the prediction of skid resistance from texture measurements using a rubber friction model. The approach, the investigations and results are presented below. To begin with, the concept of contactless skid resistance measurement shall be presented.

3. CONCEPT OF CONTACTLESS SKID RESISTANCE MEASUREMENT

The traction between tire and road pavement, amongst other things, is depending on five major influencing factors: 1) the vehicle (axle load distribution, split-up of brake power, center of gravity, wheel alignment etc.), 2) the tire (dimension, construction, material, tread depth, tread design, inflation pressure, tire temperature etc.), 3) the driving mode (braking, acceleration, cornering, speed, ambient temperature etc.), 4) the surface conditions (dry, wet, water depth, contamination, snow, ice etc) and 5) the pavement (material, microtexture, macrotexture, drainage capacity etc.).

Despite of the numerous influencing factors the typical deceleration curve of an ABS braking test on a wet road reveals a rather “simple” characteristic: after a short transition time a phase of nearly constant deceleration is reached. Neglecting air-, rolling- and climbing resistance as well as the influence of rotating masses of wheels, engine and transmission and assuming that the traction potential at the front and rear axle is fully exploited we could draw a direct connection between the deceleration reached and the traction potential of the road/vehicle combination. Indeed, the traction potential would reduce to $\mu_{wet,ABS} \approx a/g$ with “a” being the deceleration and “g” the acceleration of gravity. We can go further and notice that in this particular case the complex dynamic system can be reduced to a single mass or rather a rubber block sliding on the pavement surface.

This analogy brings us to the idea that the traction potential of a pavement - alias its skid resistance - could be calculated by means of a rubber friction model. In a further step this would lead to the following concept of contactless skid resistance measurement (Figure 5): 1) measurement of the pavement texture by means of an optical measuring system and 2) calculation of the skid resistance based on the measured texture by means of a rubber friction model.

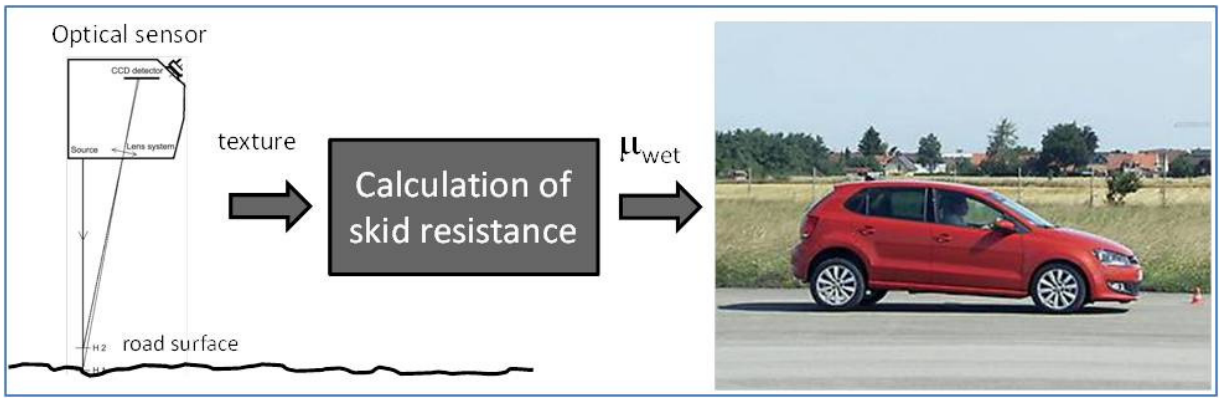

Figure 5 Concept of contactless skid resistance measurement

4. RUBBER FRICTION

Rubber friction is the predominant physical phenomenon behind skid resistance measurements. It involves several components: 1) the hysteretic component which results from internal friction of the rubber. During sliding over a rough surface the asperities exert oscillating forces on the rubber resulting in energy dissipation due to internal damping of the rubber; 2) the adhesion component which results from attractive binding forces between the rubber surface and the substrate. It is important only for clean, smooth surfaces and small sliding velocities. Persson *(31,32)* attributes adhesion friction to the roughness of the substrate as well and argues that even smooth surfaces (like glass) are not smooth on nanoscales. He showed that, due to the low elastic modulus, the interfacial free energy forces the rubber to fill out the cavities on a nano-scale, leading to oscillating forces on the rubber during sliding. Küppel and Heinrich *(33,34)* adopted this view of “adhesion induced hysteretic friction” in their theory of rubber friction; 3) the cohesion component of rubber friction which represents the energy required to produce new surfaces. It is associated with grooving of the rubber and abrasive wear; 4) the viscous friction component which arises from shearing of a viscous layer between tyre and road surface. It can occur only on wet roads.

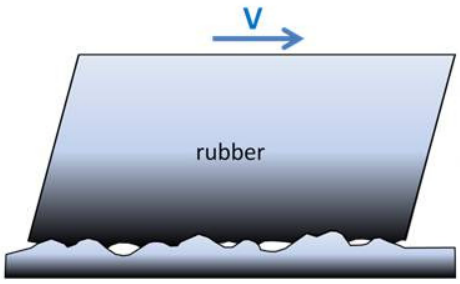

Figure 6 Tread rubber block sliding over a pavement surface

Consider a smooth tread block sliding over a rough rigid substrate (Figure 6). The friction that can be generated depends on three major influencing factors: 1) the texture in the contact patch, 2) the material behavior of the rubber (i.e. its viscoelastic and thermal properties), and 3) the "loading" conditions, like the nominal contact pressure, the ambient temperature and the sliding velocity.

4.1 DESCRIPTION OF THE PAVEMENT TEXTURE

The contact only occurs on top of the stones. Stones are broken material exhibiting a "fractal" appearance with roughness on many length scales. Wavelengths from several millimeters down to a few micrometers govern hysteresis friction. Many road surfaces exhibit self-affine properties, i.e. they "look the same" when studied under different magnifications (different in scale and different in lateral and vertical direction).

The two-dimensional power spectral density (PSD) can be used to describe the wavelength- or frequency dependency of the texture. It is defined

$$C(q) = \frac{1}{(2\pi)^2} \int d^2 x \, \langle h(\boldsymbol{x}) h(\mathbf{0}) \rangle e^{-iq\boldsymbol{x}} \qquad (1)$$

Here, h(**x**) is the surface height measured from an average plane with **x** = (x,y) and ⟨h⟩=0. The statistical properties of the texture are assumed to be isotropic so that C(q) only depends on the magnitude q = $|\mathbf{q}|$ of the wavevector **q**.

The power spectral density of self-affine surfaces follows a power law

$$C(q) \sim q^{-2(H+1)} \qquad (2)$$

where H is the Hurst exponent. The Hurst exponent is related to the fractal dimension D_f via H = 3 - D_f. The power law corresponds to a linear shape when displayed in a log-log scale. An example of a power spectral density typical of a road surface is shown in Figure 7.

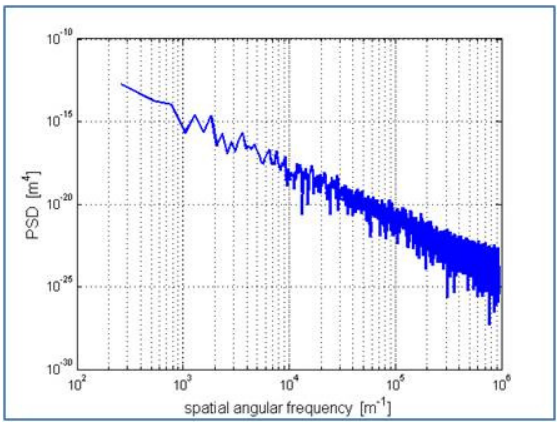

Figure 7 Two-dimensional power spectral density of a pavement surface

4.2 DESCRIPTION OF THE VISCOELASTIC BEHAVIOR

When a sinusoidal loading is applied to a piece of rubber a phase shift between strain and stress can be observed. The strain-stress diagram exhibits a so called hysteresis curve. The area enveloped by the hysteresis curve is a measure for the energy dissipated in the rubber during loading (Figure 8). The phase shift and ratio of stress and strain is a function of the loading frequency. This frequency-dependent viscoelastic behavior of rubber can be described by a complex elastic modulus

$$\sigma(j\omega) = E(j\omega) \cdot \epsilon(j\omega) \tag{3}$$

The complex modulus, again, can be described by a real part, E'(ω), called storage modulus, and an imaginary part, E''(ω), called loss modulus

$$E(j\omega) = E'(\omega) + j\,E''(\omega) \tag{4}$$

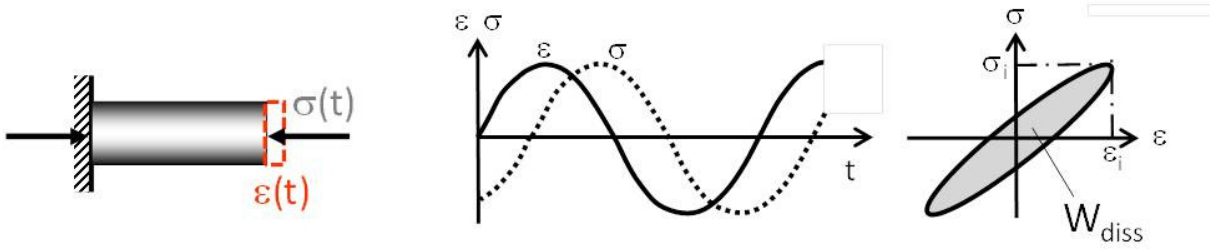

Figure 8 Stress-strain phaseshift during sinusoidal loading of a piece of rubber

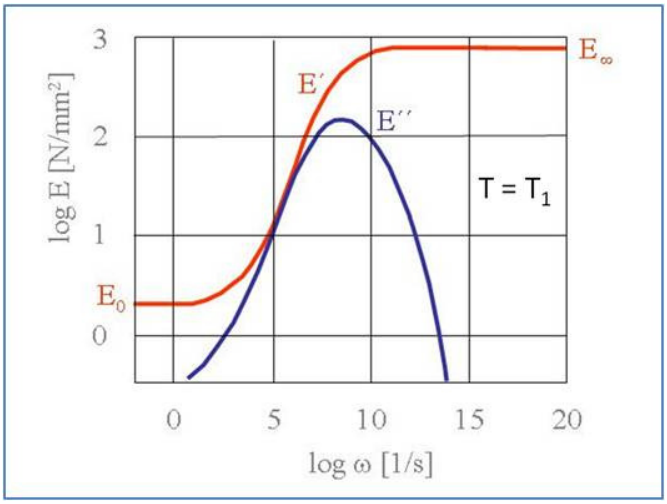

Figure 9 Influence of frequency on the modulus of rubber in terms of storage E' and loss modulus E'' (schematically)

Figure 9 shows the frequency dependent modulus of rubber (master curve) schematically in terms of its storage (red) and loss modulus (blue). For low frequencies the rubber is relatively soft. With increasing frequency it stiffens and finally reaches a maximum which in this example exceeds the low-frequency stiffness by a factor of 200 (in case of the storage modulus). In the transition zone the loss tangent (ImE/ReE) passes through its maximum (not shown). This is where the most energy is dissipated.

The complex modulus of rubber is dependent on the frequency, the temperature and the level of strain applied to the rubber. The influence of the temperature can be described by a shift of the master curve along the frequency axis. Increasing temperature leads to a shift towards higher frequencies (Figure 10). Strictly speaking this approach which is termed the time-temperature superposition principle is valid only for so-called “unfilled” natural rubber.

The temperature dependence of the elastic modulus is allowed for by the Williams-Landel-Ferry (WLF) equation *(35)*

$$\mathrm{E}(\omega, \mathrm{T}) = \mathrm{E}(\omega a_{\mathrm{T}}/a_{\mathrm{T_0}}, \mathrm{T_0}) \tag{5a}$$

with

$$\log_{10}(a_T) = \frac{-8.86 \cdot (T - T_g - 50)}{51.5 + T - T_g} \tag{5b}$$

The shift factor a_T determines the shift of the master curve towards increasing frequencies for increasing temperatures. It is valid for temperatures T higher than the glass transition temperature, which was set to Tg.= -53°C.

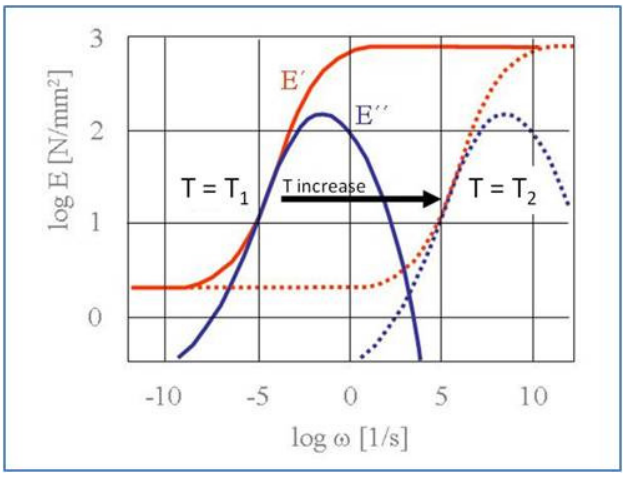

Figure 10 Influence of temperature on the modulus of unfilled natural rubber (schematically)

The modulus of elasticity is strongly dependent on the strain as described in *(36)*. The dependency on strain can be described by the so-called Kraus model *(37)*.

4.3 HYSTERESIS FRICTION MODEL ACCORDING TO PERSSON

In recent years extensive work has been done, namely by Persson, Klüppel and Heinrich, on mathematical models which allow to quantitatively determine the kinetic friction coefficient of rubber sliding against a hard, rough substrate *(31-34)*. The theories emphasize the hysteresis and adhesion component of rubber friction.

Both models, Persson's model and the model of Heinrich and Klüppel, have a physical foundation and need input information about the complex modulus of the rubber, the statistical roughness of the substrate, the contact pressure, sliding speed and temperature. The general approach is quite similar. However, Heinrich and Klüppel use a two-dimensional contact model based on the theory of Greenwood and Williamson *(38)* which they extended to multiple-scale roughness surfaces while Persson developed a new three-dimensional contact mechanics theory *(39)* which takes into account how the rubber, on each length scale, is able to follow the hard substrate. Both models consider the surface roughness on multiple length scales and thus need the viscoelastic properties of the elastomer to be known over a wide frequency range. The predictive capabilities of both models have been investigated in *(40)* by comparing the results with friction experiments.

The model that we used for the prediction of skid resistance is based on the theory of Persson *(31,32)*. The coefficient of friction according to Persson is proportional to an integral containing three major factors

$$\mu \sim \int_{q_L}^{q_H} C(q)\, P(q)\, E''(q)\, q^3 dq \tag{6}$$

Here, q is the spatial angular frequency corresponding to the wavelength $\lambda=2\pi/q$. q_L is the lower integration limit where L is of order the length of a tread block. q_1 is the upper cut-off frequency corresponding to a short distance cut-off wavelength which is depending on the operating conditions such as road contamination, wet or dry friction, measuring velocity and amount of water that has to be expelled from the interface. For dry friction the short distance wavelength can be of order one micrometer. However, surface contamination like dust and rubber particles will determine the smallest wavelength since the rubber cannot penetrate into surface cavities smaller than the typical particle diameter *(32)*. On a wet surface the short distance cut-off wavelength is determined by the smallest asperities which can penetrate the water film and the size of water "pools" trapped in small surface cavities.

C(q) denotes the two-dimensional power spectral density (PSD) of the pavement surface and E''(q) the loss modulus of the rubber. P(q) is the frequency-dependent contact function.

The contact function P(q) is defined as the ratio of real and nominal (macroscopic) area of contact, A_0, *where the surfaces are considered smooth on spatial frequencies higher than q*:

$$P(q) = \frac{A(q)}{A_0} \tag{7}$$

The real contact area A(q) normally is only a fraction of the macroscopic contact area because contact only occurs on the top of the surface asperities. The top of an asperity, in turn, would reveal many small-scale asperities if observed under magnification which in turn would exhibit even tinier asperities. This leads to the fact that the real area of contact becomes smaller and smaller the higher the magnification we use to study it (Figure 11). P(q) accounts for this scale- or frequency dependent fractal behavior. An example of a contact function is given in Figure 12.

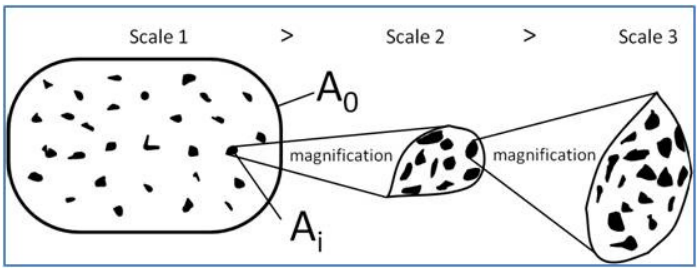

Figure 11 Real area of contact in dependency of the magnification under which it is studied

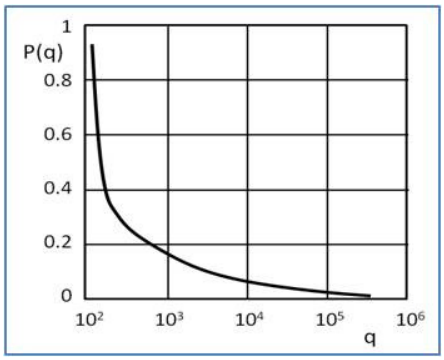

Figure 12 Example of a contact function P(q)

Physically, the contact function is determined by the texture in the contact area C(q), the material behaviour of rubber (magnitude of the elastic modulus $|E(qv\cos\phi)|$ and Poison's ratio, ν) and the "loading" conditions (nominal contact pressure, σ_0, and sliding velocity, v). It can be expressed by

$$P(q) = \frac{2}{\pi}\int_0^\infty dx \frac{\sin x}{x} \exp\left(-x^2 G(q)\right) \tag{8}$$

where

$$G(q) = \frac{1}{8}\int_{q_L}^{q} dq q^3 C(q) \int_0^{2\pi} d\phi \left| \frac{E(q\mathrm{v}\cos\phi)}{(1-\nu^2)\sigma_0} \right|^2 \tag{9}$$

C(q) denotes the two-dimensional power spectral density (PSD) of the pavement surface. Again, q is the spatial angular frequency or magnitude of the wave vector **q** = (q_x,q_y) = (qcosϕ,qsinϕ) corresponding to the wavelength λ=2π/q. Via the sliding velocity v, frequencies ω = qvcosϕ are excited which act on the tread block and depend on the sliding direction which is given by the angle ϕ between sliding direction and particular wave vector. Poisson's ratio, ν, can be set to 0.5 for rubber.

As mentioned above the texture power spectral density C(q) contains a broad band of amplitudes and frequencies. The part of it which comes into contact and determines the hysteresis losses, is

$$C_{eff}(q) = P(q) \cdot C(q) \tag{10}$$

This part of the texture penetrates the rubber and causes hysteresis losses in a broad band of excitation frequencies covering several length scales from (typically) several micrometers to several millimetres.

The hysteresis losses in each frequency band need to be summarized to give the total energy loss during sliding. The energy dissipated related to the energy used to establish the contact results in the expression for the coefficient of friction

$$\mu_k = \frac{1}{2}\int_{q_L}^{q_1} dq q^3 C(q) P(q) \int_0^{2\pi} d\phi \cos\phi \,\mathrm{Im}\frac{E(q\mathrm{v}\cos\phi)}{(1-\nu^2)\sigma_0} \tag{11}$$

The so-called "flash temperature" (41) had been included in the model initially but then was omitted because it didn't produce better results.

4.4 APPLICATION OF THE RUBBER FRICTION MODEL

Two skid resistance devices have been modeled: a laboratory device called Wehner/Schulze (W/S) machine which corresponds to a blocked-wheel braking test at a speed of 60 km/h and the ViaFriction® device of ViaTech AS, a device developed for road and airfield monitoring purposes which measures the skid resistance under controlled longitudinal slip and corresponds to ABS braking conditions. Both devices measure the skid resistance under wet conditions.

Because road surfaces are relatively rough and both measuring devices operate under wet conditions and comparatively high sliding velocities the adhesion component can be neglected and hysteresis be considered to be the dominating friction mechanism. The following assumptions have been made for the friction model: 1) the frictional process generated by the skid resistance measuring devices can be described by a steady-state process characterized by

an average sliding velocity, 2) the steady-state process is characterized by an “operating” temperature of the rubber in the vicinity of the contact zones which determines its viscoelastic properties, 3) the water acts as a coolant and ensures moderate tire temperatures compared to dry friction, 4) the contact conditions correspond to the boundary lubrication regime where in parts dry contact can be established, 5) hysteresis is the dominating friction mechanism, 6) adhesion can be neglected due to sliding velocities, pavement roughness and water film, 7) viscous effects are insignificant compared to hysteretic effects, 8) the water acts as a low-pass filter limiting the wavelengths the tire can follow in the high frequency range (sealing and expulsion constraints).

For lack of information about the rubber properties we used measured master curves of an actual tread rubber which were provided to us by a major tire manufacturer. The temperature dependence is allowed for by the Williams-Landel-Ferry equation knowing that the equation should be restricted to unfilled rubbers. For lack of appropriate information though and as a first attempt to explore the potential of the theory of rubber friction for contactless skid resistance prediction we used this approach assuming that for an appropriate frequency band - temperature constellation a behavior similar to that of the respective measuring rubbers could be found. The results seem to confirm this assumption. Nevertheless, further work should be founded on a better empirical basis.

The master curves we used are shown in Figure 13 in terms of the storage (G’) and loss modulus (G’’). They apply to a temperature of 20°C and a strain of 0.2 %. However, the strain involved in skid resistance measurement (e.g. W/S) is much higher. 8 % is considered a more realistic magnitude for the tire-road contact *(32,40)*. The strain effect on the rubber we used is shown in Figure 14, measured at an excitation frequency of 10 Hz. The solid line is the so-called Kraus model *(37)* fitted to the data. For our calculations we assumed that a characteristic strain of 8 % and a softening effect according to Figure 14 can be applied to the whole frequency range relevant to skid resistance (in our case about 10^3 to 10^6 Hz).

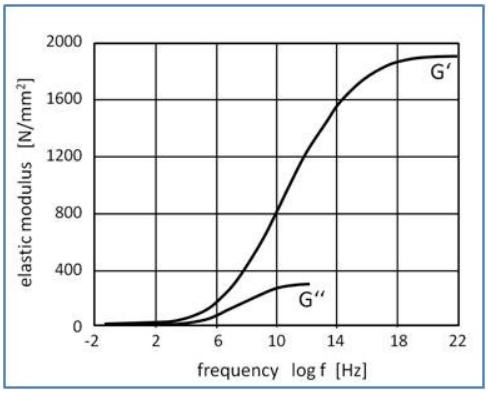

Figure 13 Measured storage (G’) and loss modulus (G’’) used for the rubber friction model (20°C, 0.2%)

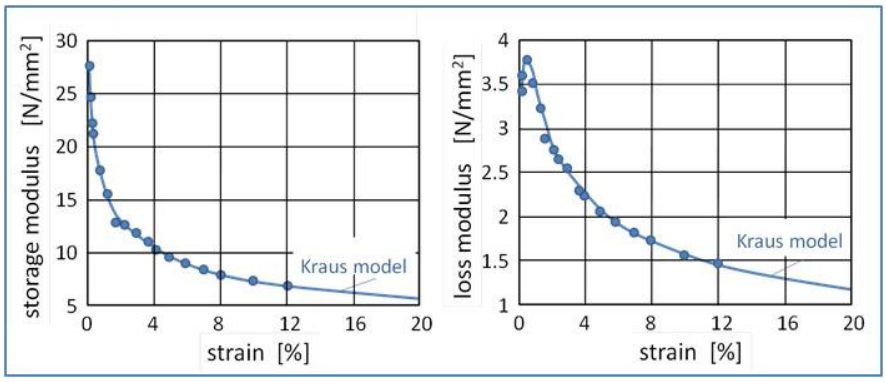

Figure 14 Measured strain dependence on storage and loss modulus for 10 Hz excitation frequency (20°C)

Table 1 contains the parameter settings for the rubber friction model. The best agreement between calculated and measured friction coefficients was obtained with a background temperature (in the rubber) of 57 °C for the Wehner/Schulze device and 47 °C for the ViaFriction® device and wavelengths considered between 20 µm and 25 mm. The calculations were based on the "linearized" power spectral density which means that the PSD in the log-log scale was fitted by a straight line. Two different fitting procedures were applied: for the ViaFriction® device all wavelengths between 20 µm and 1 mm were used to determine the straight-line fit. For the Wehner/Schulze device all wavelengths between 60 µm and 1 mm were used to determine the straight-line fit. This means that wavelengths between 20 micrometer and 25 millimeter were included in the calculation of the friction coefficient, however, wavelengths between 20 micrometer and 1 mm in the case of the ViaFriction® device and between 60 micrometer and 1 mm in case of the Wehner/Schulze device were considered decisive for the friction produced.

Table 1 Parameter settings for the rubber friction model

Parameter Settings	
Considered wavelength range	20 µm to 25 mm
Contact pressure	0.2 N/mm^2
Poisson's ratio	0.5
Average strain	8 %
Sliding velocity	60 km/h (Wehner/Schulze)
	12 km/h (ViaFriction®)
Rubber temperature in the contact zone	57 °C (Wehner/Schulze)
	47 °C (ViaFriction®)
Wavelengths treated decisive for the friction	60 µm to 1 mm (W/S)
	20 µm to 1 mm (ViaFriction®)

5. EXPERIMENTAL APPROACH

The Wehner/Schulze (W/S) device (Figure 15a) was designed to simulate accelerated wear on road surface samples and measure the skid resistance before and after the accelerated testing. For the purpose of our investigation only the skid resistance measuring unit was used. It consists of a rotating head equipped with 3 rubber pads which are arranged equiangular around a metal rim (Figure 15b). For the skid resistance measurement the head is lifted from the pavement sample and accelerated to a rim speed of 100 km/h. When the desired speed is reached the water supply is activated and the rotating head released. It drops onto the pavement sample where it is decelerated due to the friction between rubber pads and specimen. The friction is recorded as a function of speed and the friction coefficient at a speed of 60 km/h denoted the Wehner/Schulze friction coefficient, $\mu_{WS,60}$. The nominal contact pressure is 0.2 N/mm^2 corresponding to a passenger car tire.

Figure 15 Wehner/Schulze device: (a) overall view; (b) skid resistance measuring unit

The other skid resistance measuring device which has been modeled is the ViaFriction® device by ViaTech AS, Norway. It consists of a towing vehicle containing a water tank (Figure 16a) and a trailer fitted with the ViaFriction® measuring unit (Figure 16b). The device can be operated in constant or variable slip mode and, in our case, measured the longitudinal friction coefficient under wet conditions (0.5 mm water film). For our purpose a constant slip of 20 % and a measuring speed of 60 km/h were chosen. The nominal contact pressure of the slick tire (ASTM RL2, 4.00-8NHS) can be assumed to be similar to that of a passenger car tire.

Figure 16 ViaFriction® device: (a) overall view; (b) ViaFriction® measuring unit

In order to validate the contactless skid resistance measurement the surface texture was measured under laboratory conditions by a chromatic white light sensor (Figure 17a). The sensor features a lateral resolution of 1-2 micrometer and a vertical resolution of 20 nanometer. For our investigations we limited the lateral resolution to 3.3 micrometers.

Because of the circular path of the Wehner/Schulze skid resistance measurement we measured the texture within or near the path of the Wehner/Schulze device. The locations where the friction was measured can be seen from Figure 17b. 12 profiles were measured in the path of the Wehner-Schulze device. Based on these 12 profiles the one-dimensional power spectral density characterizing the sample texture was calculated. The one-dimensional PSDs where then converted to two-dimensional PSDs according to *(42)* assuming isotropic surface roughness.

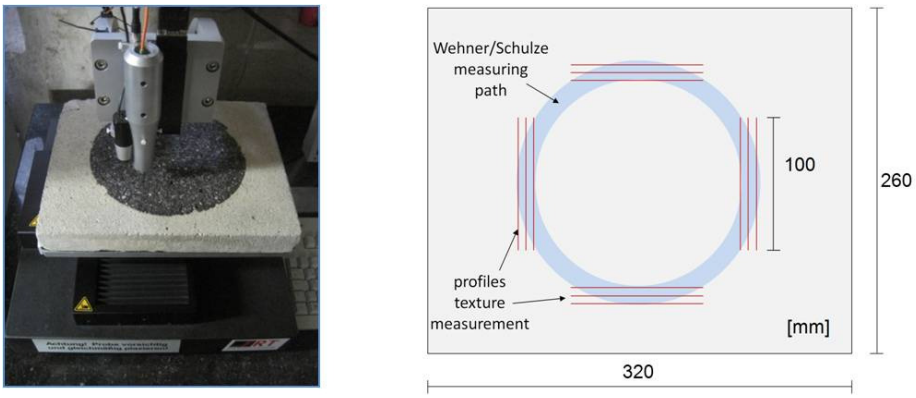

Figure 17 (a) Chromatic white light sensor; (b) location of the profile measurements

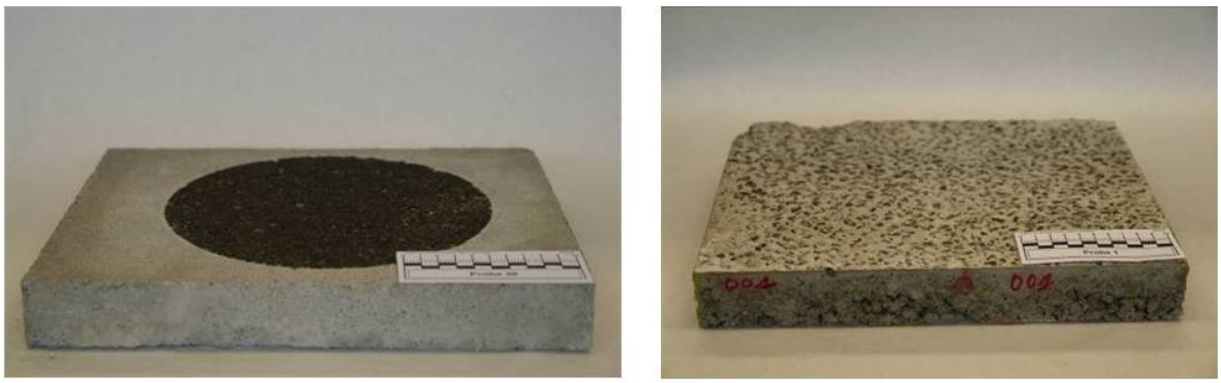

Figure 18 Examples of specimens: asphalt core and laboratory sample (concrete)

For comparison with the Wehner/Schulze device 33 different surfaces have been tested (Table 2). 13 of them were washed concrete slabs made in the laboratory exhibiting different maximum aggregate sizes (8 and 11 mm) and different polishing treatments. 20 of them were asphalt cores obtained from actual road surfaces and parking lots comprising maximum aggregate sizes between 8 and 11 mm. Examples of the specimen are shown in Figure 18. Except for one

sample which was a SMA all of them were asphalt concrete (AC) pavements. Two samples per surface were available for testing on average. The surfaces cover a wide range of friction coefficients from low-µ to high-µ roughness. Note that a Wehner/Schulze friction coefficient of around 0.6 marks a high-µ pavement because of the high sliding velocities and temperatures involved.

Table 2 Surface samples tested for the comparison with the Wehner/Schulze machine

No.	$\mu_{WS,60}$ measured	$\mu_{WS,60}$ Theory	sample size	surface example	origin/details	
1	0,43	0,42	2	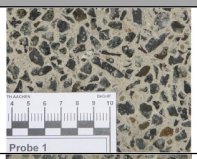	Exposed aggregate concrete, Gabbro 0/11mm	laboratory sample, initial state
2	0,62	0,61	2			laboratory sample, sandblasted
3	0,42	0,44	2			laboratory sample, polishing stage 1
4	0,43	0,41	2			laboratory sample, polishing stage 2
5	0,45	0,44	2		Exposed aggregate concrete, Gabbro 0/11mm	laboratory sample, initial state
6	0,64	0,64	2			laboratory sample, sandblasted
7	0,47	0,47	2			laboratory sample, polishing stage 1
8	0,45	0,48	2			laboratory sample, polishing stage 2
9	0,36	0,31	2		Exposed aggregate concrete, Gabbro 0/11mm	laboratory sample, initial state
10	0,53	0,52	2			laboratory sample, sandblasted
11	0,32	0,34	2			laboratory sample, polishing stage 1
12	0,37	0,38	2			laboratory sample, polishing stage 2
13	0,24	0,25	4	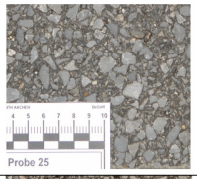	AC Greywacke 0/11mm	Aachen, Goethestraße 13
14	0,20	0,22	2		AC Greywacke 0/11mm	Aachen, Boxgraben 22, initial state
15	0,18	0,17	2			Aachen, Boxgraben 22, polishing stage 1
16	0,19	0,20	2			Aachen, Boxgraben 22, polishing stage 2
17	0,17	0,20	4		AC Greywacke 0/8mm	Aachen, Lütticher Straße 21
18	0,30	0,28	1			Aachen, Wallstraße 57
19	0,30	0,29	2			Aachen, Lütticher Straße 56, right lane
20	0,24	0,23	4			Aachen, Lütticher Straße 56, left lane
21	0,28	0,28	1		AC Greywacke 0/8mm	Aachen, Boxgraben 32
22	0,28	0,28	1			Aachen, Lütticher Straße 21, bicycle lane
23	0,33	0,35	3			Aachen, Rüd. Ring, road surface
24	0,50	0,55	3			Aachen, Rüd. Ring, adjacent areas
25	0,36	0,38	1		AC Basalt 0/11mm	Aachen, Madrider Ring
26	0,30	0,27	2		SMA Greywacke 0/11mm	Eschweiler (36+37), left and right lane
27	0,28	0,26	1		AC Greywacke 0/11mm	Aachen, parking lot, coarse aggregate
28	0,31	0,29	2			Aachen, parking lot, fine aggregate
29	0,32	0,30	2		AC Greywacke 0/8mm	Aachen, parking lot
30	0,36	0,35	2			Aachen, parking lot
31	0,33	0,34	2			Aachen, parking lot
32	0,35	0,33	1			Aachen, Schleidener Straße
33	0,46	0,47	4		Gabbro 0/11mm	laboratory sample, Exposed aggregate concrete

The concrete slabs made in the laboratory were subjected to sandblasting and subsequent polishing in two stages in order to enlarge the sample size. The respective surfaces are denoted accordingly in Table 2. The polishing was performed by the ARTe (Aachen Rafeling Tester) shown in Figure 19. It features a pair of passenger car wheels which are moved across the specimen surface in a combined rotational and translational motion. The tires of dimension 165/75 R14 are operated with a tire pressure of 2 bar. The load is 1500 N. A mixture of polishing agents and water was applied to accelerate the wear.

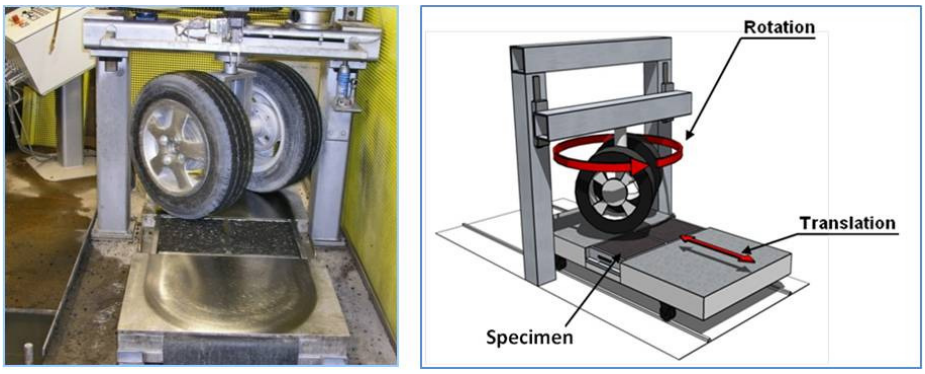

Figure 19 Aachen Rafeling Tester (ARTe)

Table 3 Surface samples tested for the comparison with the ViaFriction® device

No.	Internal No.	$\mu_{VF60-20}$ measured	$\mu_{VF60-20}$ calculated	sample size	pavement	details/origin
1	301/302	0,71	0,73	2	SMA 0/8 Granite Greywacke	B56 dir. Puffendorf; Station 1+200 left, section 15.2
2	303/304	0,65	0,66	2	SMA 0/8 Granite Greywacke	B56 dir. Aldenhoven; Station 1+200 right, section 15.2
3	305/306	0,78	0,78	2	SMA 0/11 Granite Greywacke	B55 dir. Elsdorf; Station 2+400 right, section 5
4	307/308	0,68	0,68	2	AC 0/11 Granite Diabase	L366 dir. Hompesch; Station 0+600 right, section 1
5	309/310	0,68	0,66	2	AC 0/11 Granite Diabase	L366 dir. A44; Station 0+600 left, section 1

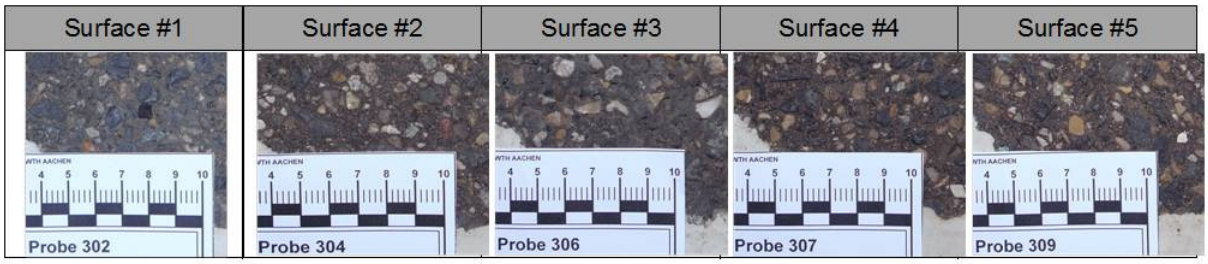

Figure 20 Surfaces analyzed for the comparison with the ViaFriction device (exemplary)

For comparison with the ViaFriction® device unfortunately only 5 different surfaces could be tested for lack of permission to drill cores on public roadways. Besides that, we could not resort to the surfaces from Table 2 because the respective drill cores were taken before the ViaFriction® device was available. The surfaces, three of them SMA and two AC pavements, were very homogeneous regarding their skid resistance. Two cores per surface could be taken. Data on the location and type of pavement as well as on the measured and calculated friction coefficients are given in Table 3. Examplary photos of the surfaces are shown in Figure 20.

6. RESULTS AND DISCUSSION

The comparison of measured and calculated friction coefficients is shown in Figure 21 for the W/S machine. The macroscopic contact pressure was set to σ_0 = 0.2 N/mm^2, Poisson's ratio to ν = 0.5 and the maximum and minimum wavelengths to 25 mm and 20 micrometer respectively. The best agreement between calculated and measured friction coefficients was obtained with a background temperature (in the rubber) of 57 °C and a linear fit of the power spectral density in the log-log scale under the premise that only the wavelengths between 1 mm and 60 micrometer determine the fit. This means that wavelengths between 25 mm and 20 micrometer are included in the calculation of the friction coefficient, however, wavelengths between 1 mm and 60 micrometer are considered decisive. As can be seen from the graph the agreement between measured and calculated friction coefficients is very good (R^2 = 0.97).

The blue dots mark the mean values of the 33 surfaces, the white dots the single values (70 in total). At the waist the 95 % prediction interval is +/- 0.04 and the variance 0.02 units of friction.

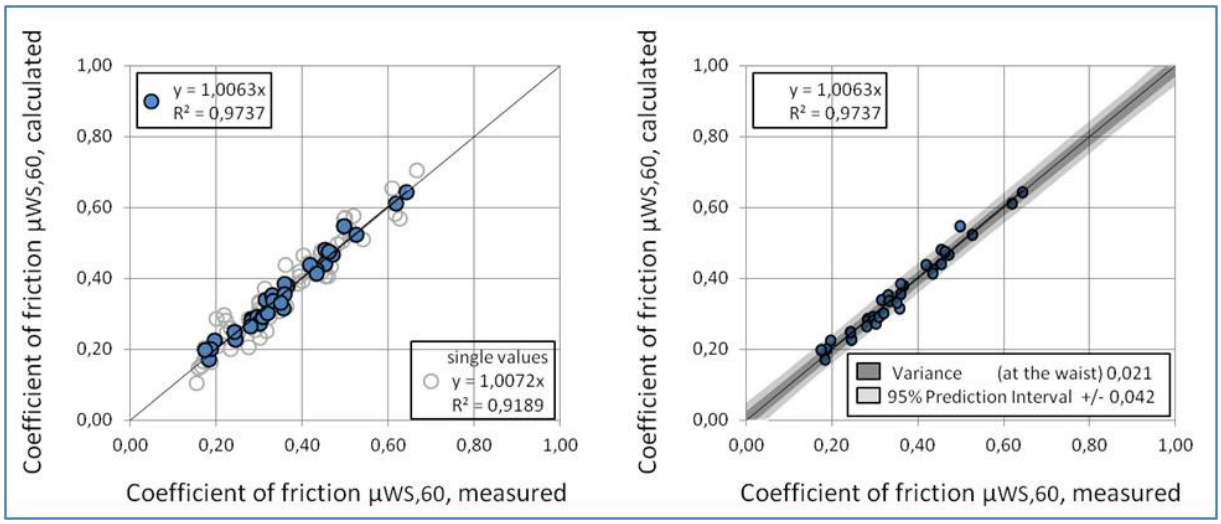

Figure 21 Wehner-Schulze machine: Comparison of measured and calculated friction coefficients

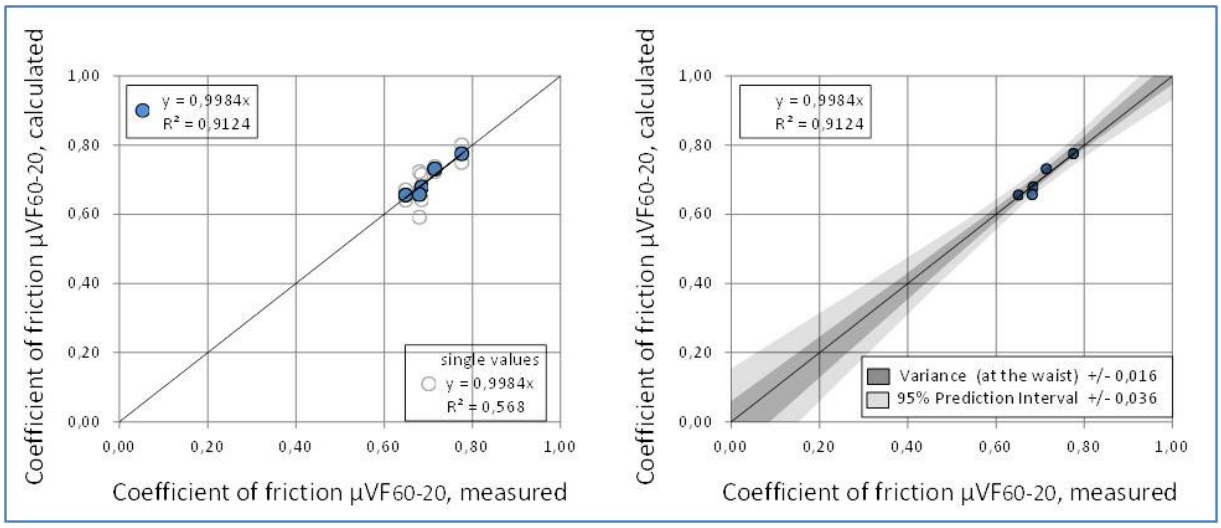

Figure 22 ViaFriction® device: Comparison of measured and calculated friction coefficients

Figure 22 shows the comparison of measured and calculated friction coefficients for the ViaFriction device. As with the W/S machine, the macroscopic contact pressure was set to σ_0 = 0.2 N/mm^2, Poisson's ratio to ν = 0.5 and the maximum and minimum wavelengths to 25 mm and 20 micrometer respectively. The best agreement between calculated and measured friction coefficients was obtained with a background temperature of 47 °C and a linear fit of the power spectral density in the log-log scale under the premise that the wavelengths between 1 mm and 20 micrometer determine the fit. This means that, unlike in the case of the W/S machine, wavelengths from 1 mm down to 20 micrometer were considered decisive for the coefficient of friction of the ViaFriction® device. Despite the small number of samples good agreement between measured and calculated friction coefficients could be found (R^2 = 0.91). The blue dots mark the mean values of the 5 surfaces, the white dots the single values (10 in total). At the waist the 95 % prediction interval is +/- 0.04 and the variance 0.02 as was found for the W/S machine.

Both results, the findings for the W/S machine and the ViaFriction device, seem to be quite reasonable. 60 °C is a typical tire temperature during driving on a dry road; on a wet road due to liquid cooling the temperature is typically around 30 °C *(43)*. Thus, rubber temperatures of 57 °C (W/S) and 47 °C (ViaFriction) can be expected as an average in the vicinity of contact spots under wet sliding conditions. Furthermore, it is reasonable that the friction process in the W/S machine is associated with higher temperatures than the friction process in the ViaFriction device because of the higher sliding velocities involved (100 – 0 km/h compared to 12 km/h). Although the amount of water involved in the W/S friction process seems to be higher than that involved in the ViaFriction device considerably more heat is generated in the W/S machine.

Another point that seems reasonable is that for the ViaFriction device the decisive wavelength range extends to smaller wavelengths than for the W/S machine (20 micrometer compared to 60 micrometer). The reason, again, is the different sliding velocity. Because of the lower sliding velocity the ViaFriction rubber is able to follow smaller wavelengths. The W/S machine on the contrary is associated with higher velocities (up to 100 km/h), smaller expulsion periods and possibly more water volume involved in the friction process which has to be expelled.

Due to both, the temperature (as a result of the sliding velocity) and the influence of the water, the friction which can be generated by the W/S machine is significantly lower than the one that can be generated by the ViaFriction device.

These conclusions, however, are based on the assumption that both devices were equipped with the same rubber (see chapter 4) which, in fact, is not the case. So, in reality, the different friction levels are influenced by the (different) rubber properties as well.

Although the rubber friction model for the ViaFriction device could be applied only to a few surfaces the results for both applications, the W/S machine and the ViaFriction device, seem very promising.

7. SUMMARY AND CONCLUSION

In the paper a concept of contactless skid resistance measurement is presented. It consists of two components: 1) measurement of the pavement texture by means of an optical measuring system and 2) calculation of the skid resistance based on the measured texture by means of a rubber friction model. We described the basic assumptions underlying the theoretical approach and presented the model based on the theory of Persson. Two skid resistance measuring devices were chosen to prove the theoretical approach: one laboratory device called Wehner/Schulze (W/S) machine which corresponds to a blocked-wheel braking test and the ViaFriction® device of ViaTech AS which measures the skid resistance under controlled longitudinal slip and corresponds to ABS braking conditions. We described the measurement devices and experiments conducted. For texture measurement we used a chromatic white light sensor.

The results are very promising although in the case of the ViaFriction® device only a few surfaces could be tested. A close relationship between measured and predicted friction coefficients could be found. The 95 % prediction interval is +/- 0.04 and the variance 0.02. Thus, a strong indication could be provided by the investigations that skid resistance could be measured without contact in the future. As a next step the contactless skid resistance measurements shall be extended from laboratory environment to in-situ applications. This involves the setup of a new optical sensor and according data processing which is to be optimized in extensive testing on the road.

REFERENCES

[1] Dunford, A. Measuring skid resistance without contact. 2009-2010 progress report, Published Project Report PPR 538, Transport and Research Laboratory, Wokingham, England, 2010

[2] Dunford, A, A. Ruff, and R. Whiteoak. Measuring skid resistance without contact, 2007-2008 progress report, Published Project Report PPR 378, Transport and Research Laboratory, Wokingham, England, 2008

[3] Dunford, A. Measuring skid resistance without contact; 2006-2007, Published Project Report PPR 315, Transport and Research Laboratory, Wokingham, England, 2008

[4] Meegoda, J.N. Non-contact skid resistance measurement, final report, December 2009, New Jersey Institute of Technology, University Heights, Newark, NJ 07102-1982

[5] Xie, J., R. Liu, and B. Michalk, Automatik skid number evaluation using texture laser measurement, International Conference on Networking, Sensing and Control, Sanya 6-8 April 2008, ICNSC 2008, pp. 37-42

[6] Cigada, A., F. Mancosu, S. Manzoni, and E. Zappa. Laser triangulation device for in-line measurement of road texture at medium and high speed, Mechanical Systems and Signal Processing, Volume 24, Issue 7, October 2010, pp. 2225-2234

[7] Kebrle, J., and R. Walker, Texture measurement and friction estimation using laser data acquisition and neural networks, Proc. of the 9th WSEAS Int. Conf. on Mathematical and Computational Methods in Science and Engineering, Trinidad and Tobago, November 5-7, 2007, pp. 29-33

[8] Xiangyang, M., L. Lin, T. Nan, C. Liu, and J. Xiuhan, A laser-based system for highway pavement texture measurement, Proceedings of the Conference on Intelligent Transportation Systems, 12-15 October 2003, Vol. 2, pp. 1559-1562

[9] Goubert, L., C. Vuye, T. Jacobs, and B. Tuerlinckx, Micro/Macrotexture and Skidding Resistance, Presented at the Tire Technology Expo 2010 & Conference, 9-11 February 2010, Koelnmesse, Cologne, Germany

[10] Sabey, B.E., and G.N. Lupton, Measurement of road surface texture using photogrammetry, Report LR 57, Road Research Laboratory, UK, 1967

[11] Schonfeld, R. Skid numbers from stereo-photographs, Report RR 155, Ontario Department of Highway, 1970

[12] Ben Slimane, A., M. Khoudeir, J. Brochard, and M.-T. Do. Characterisation of road microtexture by means of image analysis, Wear 264 (2008), pp. 464-468

[13] Xie, L., X. Chu, W. Wang, and C. Chen, A stereoscopic imaging arithmetic for 3D measurement of road surface micro-texture, Proceedings of the International Conference on Transportation Engineering, July 25-27, 2009, Chengdu, China, pp. 4222-4227

[14] El Gendy, A., A. Shalaby, M. Saleh, and G.W. Flintsch, Stereo-vision applications to reconstruct the 3D texture of pavement surface, International Journal of Pavement Engineering, Vol. 12, No. 3, June 2011, pp. 263-273

[15] Wambold, J.C., J.J. Henry, and R.R. Hegmon, Evaluation of pavement surface texture significance and measurement techniques, Wear, Volume 83, Issue 2 (1982), pp. 351-368

[16] Spring III, W.C., and W.L.King, Light depolarization as a measure of pavement surface texture, Final Report, May 1974 - Mar. 1981, Naval Surface Weapons Center, Silver Spring, MD.

[17] Iaquinta, J., and A. Fouilloux, A differential scattering probe for monitoring road surfaces, Measurement Science Review, Volume 3, Section 3 (2003), pp. 107-110

[18] Kazakov, A.L. Pavement texture and its wave-scattering properties: application to light reflectance and skid resistance. In Transportation Research Record 1093 (1986), pp. 48-57

[19] Do, M.-T., P. Marsac, and Y. Delanne, Prediction of tire/wet road friction from road surface microtexture, and tire rubber properties, 5th International Symposium on Pavement Surface Characteristics SURF 2004, Toronto, Ontario, Canada, 6-10 June 2004

[20] Do, M.-T., and H. Zahouani. Influence of the road-surface texture on the speed dependency of tire/road friction, 10th International Conference Metrology and Properties of Engineering Surfaces, Saint Etienne, France, 5-7 July 2005, pp. 369-378

[21] Kane, M., and M.-T. Do. A contribution of elastohydrodynamic lubrication for estimation of tire-road friction in wet conditions, AITC-AIT 2006 International Conference on Tribology, Parma, Italy, 20-22 September 2006

[22] Zahouani, H., R. Vargiolu, and M.-T. Do, Characterization of microtexture related to wet road/tire friction, 4th International Symposium on Pavement Surface Characteristics SURF 2000, Nante, France, 22-24 May 2000

[23] Ergün, M., S. Iyinam, and A.F. Iyinam, Prediction of road surface friction coefficient using only macro- and microtexture measurements. Journal of Transportation Engineering (2005) 131, pp. 311-319

[24] Shalaby, A., and A. El Gendy, Three-dimensional pavement surface macrotexture measurements using the photometric stereo technique and applications, 6th International Symposium on Pavement Surface Characteristics SURF 2008, Portorož, Slovenia, 20-22 October 2008

[25] Ustuntas, T. Prediction of skid resistance coefficient of cement concrete roads with fuzzy logic, Civil Eingineering and Environmental Systems, Vol. 24, No. 3, September 2007, pp. 233-246

[26] Pinnington, R.J., 2009. Rubber friction on rough and smooth surfaces, Wear Vol. 267, Issue 9-10, pp. 1653-1664

[27] Kummer, H.W., Meyer, W. E., 1967. Verbesserter Kraftschluss zwischen Reifen und Fahrbahn, Ergebnisse einer neuen Reibungstheorie, ATZ 69/8, pp. 245 ff.

[28] Radó, Z., 1994. A study of road surface texture and its relationship to friction, Thesis (PhD), Pennsylvania State University

[29] Moore, D.F. The sinkage of flat plates on smooth and rough surfaces, Ph.D. Thesis, Pennsylvania State University, 1963

[30] Do, M.-T., P. Marsac, and A. Mosset, Tribology approach to predict the variation of tire/wet road friction with slip speed, 5th International Symposium on Pavement Surface Characteristics SURF 2004, Toronto, Ontario, Canada, 6-10 June 2004

[31] Persson, B.N.J. Theory of rubber friction and contact mechanics, Journal of Chemical Physics (115) 8, S. 3840-3861, 2001

[32] Persson, B.N.J. Theory of rubber friction, contact mechanics and the role of surface roughness on the adhesion of elastic solids. Presented at the 160th meeting of the Rubber Division, American Chemical Society, Cleveland, Ohio, 16-19 October 2001

[33] Klüppel, M., and G. Heinrich, Rubber friction on self-affine road tracks, Rubber Chemestry and Technology, Vol. 73, No. 578 (2000), pp. 578-606

[34] Heinrich, G., M. Klüppel, and T.A. Vilgis, Evaluation of self-affine surfaces and their implication for frictional dynamics as illustrated with a Rouse material, Computational and Theoretical Polymer Science, Volume 10 (2000), pp. 53-61

[35] Williams, M.L., Landel, R.F. and Ferry, J.D., 1955. The Temperature Dependence of Relaxation Mechanisms in Amorphous Polymers and Other Glass-forming Liquids, Journal of the American Chemical Society, Volume 77, pp. 3701-3707

[36] Payne, A.R., 1964. Strainwork dependence of filler-loaded vulcanizates, Journal of Applied Polymer Science, Volume 8, Issue 6, pp. 2661-2686

[37] Kraus, G. and Lansinger, C.M., 1992. Characterization of surface energy of carbon black surfaces and relationship to elastomer reinforcement, Kautschuk Gummi Kunststoffe 45, pp. 459-468

[38] Greenwood, J.A., and J.B.P. Williamson, Contact of nominally flat surfaces, Proceedings Royal Society of London A 6 (1966), Vol. 295, No. 1442, pp. 300-319

[39] Persson, B.N.J. Contact mechanics for randomly rough surfaces, Surface Science Reports, Volume 61 (2006), pp. 201-227

[40] Westermann, S., F. Petry, R. Boes, and G. Thielen, Experimental investigations into the predictive capabilities of current physical rubber friction theories, Kautschuk Gummi Kunststoffe, Volume 57, Nr. 12 (2004), pp. 645-650

[41] B.N.J. Persson, Rubber friction: the role of the flash temperature, Journal of Physics: Condensed Matter, Volume 18 (2006), pp. 7789-7823

[42] Carbone, G., Lorenz, B., Persson, B.N.J., Wohlers, A., 2009. Contact mechanics and rubber friction for randomly rough surfaces with anisotropic statistical properties, The European Physical Journal E, Volume 29 (2009), pp. 275-284

[43] Persson, B.N.J., U. Tartaglino, E. Tosatti, and O. Albohr, Rubber friction on wet rough substrates at low sliding velocity: the sealing effect, Kautschuk Gummi Kunststoffe, Volume 57, Nr. 10 (2004), pp. 532-537

Author Biographies

Andreas Ueckermann

Andreas Ueckermann graduated in 1987 from Technical University (TU) of Brunswick in Germany with a degree (diploma) in mechanical engineering. From 1987 to 1990 he worked as a researcher at the Institute of Vehicle Engineering at TU Brunswick. During that time he was a teaching assistant for the lecture “Vehicle Dynamics”. His research focused on road unevenness and its effects on vehicle dynamics, human health and road loading. Since 1997 he is a researcher at the Institute of Road and Traffic Engineering at RWTH Aachen University where he completed his PhD in 2004. Main research topics are the assessment of road evenness, road surface texture and its effects on skid resistance and the modeling of vehicle-road interaction.

Dawei Wang

Dawei Wang graduated in 2007 from RWTH Aachen University in Germany with a degree (diploma) in civil engineering. Since 2008 he is a research engineer at the Institute of Road and

Traffic Engineering at RWTH Aachen University. 2011 he earned a doctorate on the subject of mineralogical analysis of the aggregates regarding polishing resistance. Main research topics are road surface texture and its effects on skid resistance, prediction of urban road conditions, and the investigation of the frictional behavior of the aggregates on road surface.